Mechanism of Atmospheric CO$_2$ Fixation in the Cavities of a Dinuclear Cryptate

Morad M. El-Hendawy,[†] Niall J. English,*[,†,‡] and Damian A. Mooney[†,‡]

[†]The SFI Strategic Research Cluster in Solar Energy Conversion, School of Chemical and Bioprocess Engineering and [‡]Centre for Synthesis and Chemical Biology, University College Dublin, Belfield, Dublin 4, Ireland

ABSTRACT: Using density functional theory (DFT) methods, we have investigated two possible mechanisms for atmospheric CO$_2$ fixation in the cavity of the dinuclear zinc(II) octa-azacryptate, and the subsequent reaction with methanol whereby this latter reaction transforms the (essentially) chemically inert CO$_2$ into useful products. The first mechanism (I) was proposed by Chen et al. [*Chem.—Asian J.* **2007**, *2*, *710*], and involves the attachment of one CO$_2$ molecule onto the hydroxyl-cryptate form, resulting in the formation of a bicarbonate-cryptate species and subsequent reaction with one methanol molecule. In addition, we suggest another mechanism that is initiated via the attachment of a methanol molecule onto one of the Zn-centers, yielding a methoxy-cryptate species. The product is used to activate a CO$_2$ molecule and generate a methoxycarbonate-cryptate. The energy profiles of both mechanisms were determined, and we conclude that, while both mechanisms are energetically feasible, free energy profiles suggest that the scheme proposed by Chen et al. is most likely.
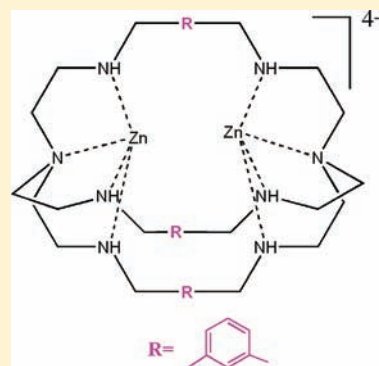
INTRODUCTION

In recent years, there has been increasing interest in the development of synthetic analogues which mimic the function of ribulose-1,5-bisphosphate carboxylase oxygenase (Rubisco);[1−33] Rubisco catalyzing the first major step of carbon dioxide fixation in nature, a conversion process to form energy-rich molecules, such as glucose. This search has become all the more tantalizing in light of the possible negative effects of anthropogenic CO$_2$ and the need to develop, long-term renewable energy resources. In the latter case, CO$_2$ being an abundant and readily accessible atmospheric gas, it can be regarded as a useful synthetic source for organic compounds, including fuels. However, its inherent thermodynamic stability and kinetic inertness poses significant challenges so as to achieve CO$_2$ activation and functionalization. The formation of coordination bonds with inert molecules is one of the most powerful and popular ways for inducing (fixing) them for subsequent reaction.[18] More specifically, in the case of CO$_2$ the challenge often encountered is the activation of the thermodynamically stable C−O bond, which has characteristics of a double bond.

Previous work has shown that, in the presence of appropriate ligand environments and electron-rich metal centers, the reduction of CO$_2$ is possible, producing carbonates, oxalates, for example.[1−17] A variety of transition metal complexes with M-OR fragments undergo insertion reactions with CO$_2$.[4,6,7,18] If R is an alkyl or aryl group, corresponding alkyl or aryl carbonate species are formed, while if R is a H atom, bicarbonate species are formed. A series of hydroxo- complexes of first-row divalent metal cations (Mn, Fe, Co, Ni, Cu, and Zn) have been found to react with CO$_2$ to form μ-carbonato-dinuclear complexes.[1] It has also been reported that zinc hydroxyl complexes can be converted to alkyl carbonate

complexes by reaction with alcohol.[2] Meanwhile, in biology, for instance, the ubiquitous Zn(II) enzyme carbonic anhydrase removes CO$_2$ from tissues in the mammalian respiratory process by inserting it into Zn−OH bonds.[3]

Recently, Nelson and co-workers have observed that the reaction of M^{2+} ions (where M^{2+} is Co^{2+} Ni^{2+}, Cu^{2+} or Zn^{2+}) with *m*-benzene-based cryptands (L) in water, and either MeOH or MeCN, produces dinuclear carbonato-cryptates [M$_2$L(μ-CO$_3$)]$^{2+}$ and dinuclear methoxycarbonate-cryptates [M$_2$L(μ-MeCO$_3$)]$^{3+}$, respectively.[4] Chen et al. have repeated these experiments in acidic solution, and obtained bicarbonate [Cu$_2$L(μ-CO$_3$H)]$^{2+}$ and methoxycarbonate species [Cu$_2$L(μ-MeCO$_3$)]$^{3+}$, respectively.[5] At present, the mechanism for the formation of the methoxycarbonate species remains unclear. Figure 1 presents the two possible mechanisms for CO$_2$ fixation and transformation into methoxycarbonate species using dinuclear zinc cryptates [Zn$_2$L]$^{4+}$. The first pathway (and referred to subsequently thus) is suggested by Chen et al., in which a CO$_2$ molecule is taken up first to form a bicarbonate species, followed by the attack by MeOH on the carbon atoms of the fixed CO$_2$ fragment.[5] As an attempt to lend credence to this mechanism, we suggest another pathway (from henceforth referred to as "the second pathway"), whereby the methoxy species is formed first by the attachment of MeOH at one of Zn cations of [Zn$_2$L]$^{4+}$, followed by interaction of CO$_2$ with the Zn-OMe bond. Although extensive studies have been conducted to study the mechanism of CO$_2$ fixation using metal−ligand complexes[10,24−31] little has been done for dinuclear metal macrocycle systems.[32,33] In view of the importance of clarifying these mechanisms, careful scrutiny of
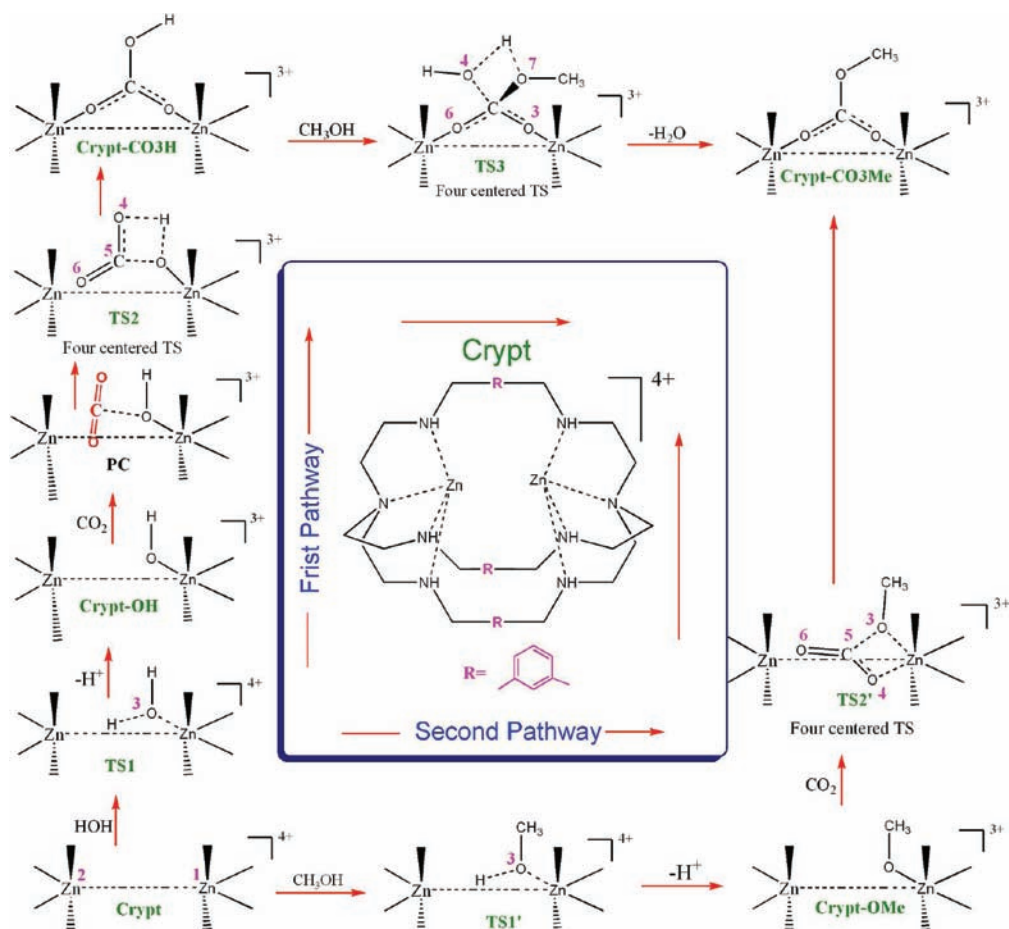
Figure 1. Two suggested reaction pathways (I and II) for activation of atmospheric CO_2 fixation into dinuclear cryptate cavity. The labeling of atoms is illustrated on the individual structures in the figure.
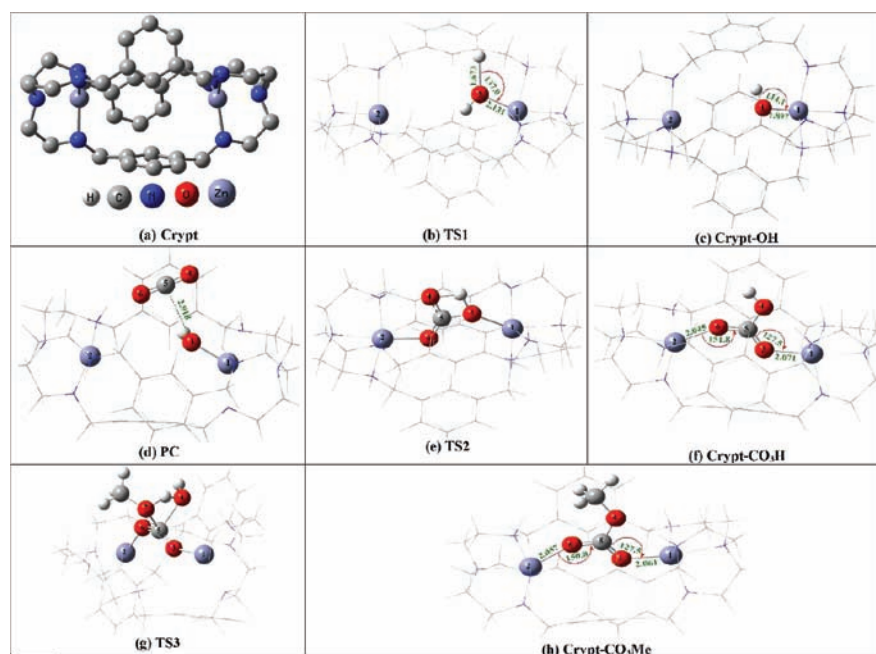
Figure 2. Optimized structures of the reactant, intermediates, transition states, and the product in the first pathway. The atomic labeling of key atoms and bond distances in Å and angles in degree are illustrated on the structures.

the validity of both mechanisms is needed (cf. Figure 1). Therefore, in this study, through the use of density functional theory (DFT), we present a comprehensive computational analysis to elucidate the possible mechanisms of methoxycar-

bonate formation by dinuclear zinc cryptates in methanolic solution, and also highlight the utility of these techniques in yielding insight in understanding catalytic mechanisms.

■ COMPUTATIONAL METHODOLOGY

All calculations were performed using Density Functional Theory (DFT) as implemented in Gaussian 09.[34] The hybrid B3LYP approach, involving the Becke exchange functional and Lee−Yang−Parr correlation functional in conjunction with Hartree−Fock exchange,[35−37] was used since it generally leads to more accurate energies.[37] Mixed basis sets were used for geometry optimization, for which Zn atoms were treated with Stuttgart/Dresden double-ζ (SDD) ECP basis sets,[38] while all-electron 6-31G(d,p) basis sets were used for the remainder of the elements in the dinuclear zinic cryptate (**Crypt**) molecule. Both minima and transition states were verified via analytical frequency calculations. Intrinsic reaction coordinate (IRC) calculations and the animation of the negative eigenvector coordinate by visualization (via GaussView 4) were utilized to verify the connections between the optimized transition states. We refined the energy and carried out population analysis by performing single-point calculations at the B3LYP/6-311++G(2d,2p) level. The thermodynamic and activation parameters were obtained at a temperature, T = 298.15 K (harmonic approximation). The electronic density was analyzed using the natural bond orbital (NBO) technique.[39] To estimate the energetic effects of a methanolic medium, as used experimentally for the fixation process,[4,5] solvation effects were calculated at the B3LYP/6-311++G(2d,2p) level using the universal solvent model, SMD.[40]

■ RESULTS AND DISCUSSION

The two, aforementioned plausible mechanistic pathways for CO_2 fixation into the cavity of dizinic cryptate in methanolic solution will be discussed here. Although, the calculations have been done both in gas and in solution, we found that the solvation effect oscillates around 2.0 kcal/mol in all cases. Thus, all presented results here include the solvation. Both mechanisms start with the **Crypt** molecule (see Figure 2 for respective optimized structures). The B3LYP-optimized structure of the **Crypt** molecule is a bis-chelating macrocyclic complex forming two connected tetrahedrons where the encapsulated zinc cations are coordinated by the three secondary amino donors (N^{second}) and the tertiary nitrogen bridgehead (N^{tr}). The structural features of the optimized species do not deviate much from that of the crystallographically derived form.[4] The average $Zn−N^{second}$ bond length equals to 2.056 Å while $Zn−N^{tr}$ bonds are higher by 0.02 Å, in good agreement with experiments.[4]

First Pathway. On the basis of our calculation (cf. Figure 2), CO_2 fixation via this route involves seven distinct chemical steps: (1) the interaction between the Crypt species and a neighboring water molecule, (2) the subsequent deprotonation of water molecule to produce the hydroxy species (**Crypt−OH**), (3) the formation of a weak associated precursor complex with CO_2 (**PC**), (4) the rearrangement into a suitable transition state (**TS2**) pushing the reaction forward, (5) the formation of a bicarbonate species (Crypt-CO_3H), (6) the MeOH attack on the bicarbonate species to form activated species (**TS3**), and (7) the subsequent formation of a methoxide carbonate species. (**Crypt-CO_3Me**). All these steps will be discussed below in a bit more detail.

Step (1 and 2): Attack of an H_2O Molecule on One of the Zn Ions and Subsequent Deprotonation. The reaction starts with the attack of a water molecule on one of the four coordinated Zn cations (Zn1) of the initial reactant (**Crypt**) to form a penta-coordinated Zn center, with subsequent deprotonation of the water molecule to form a hydroxyl

species (**Crypt−OH**). This has been achieved through the formation of a transition state, labeled **TS1,** as shown in Figure 2. A new (Zn1−O3) bond is formed and the O3−H bond is broken. For **TS1**, Zn1−O3 and O3−H distances are 2.131 and 1.501 Å, respectively. The formation of **Crypt−OH** is found to be endergonic with value of 39.6 kcal/mol. This step is thermodynamically unfavorable as the energy of the product is significantly higher than the energy of the reactant. The relative activation energy of **TS1** for this reaction through the transition state **TS1** is 72.0 kcal/mol.

An important observation is made regarding the Zn···Zn distance during the formation of hydroxyl species. Here, although the Zn···Zn distance of **Crypt** species is 6.841 Å, it reduces to 6.341 Å in the case of **TS1**, with a further reduction in the hydroxyl species to 6.264 Å. This, of course, incurs a significant energetic penalty. This reduction in the interatomic distance between the Zn atoms is attributed to attraction with respect to proximity with the water's oxygen atom. This can been seen from natural population analysis before and after forming the hydroxyl species, wherein the charge on Zn1 and Zn2 of the **Crypt** are 1.415 e and 1.420 e, respectively, and they decrease to 1.355 and 1.404 e, respectively, after inclusion of the −OH group in the interatomic distance between Zn atoms.

Step (3): Formation of Weak Associated Precursor Complex with CO_2. The second step in the first pathway is the formation of a weakly associated precursor complex (**PC**) from the reactants at infinite separation. The CO_2 molecule locates on the mirror plane perpendicular to the Zn−OH plane, as depicted in Figure 2 (see "PC" panel). The closest contact between the hydroxyl oxygen (O_3) and the CO_2 carbon atom ($C5$) is shorter than the van der Waals separation, that is, 2.918 Å.[41] In addition, the CO_2 molecule deviates little from linearity (average 175°), indicating its somewhat limited interaction with the already-complexed cryptate. The **PC** formation was found to be enthalpically favorable by 5.4 kcal/mol. Also, as expected, the association led to loss in entropy of 39.4 kcal/mol-K.

Step (4 and 5): Structural Rearrangement and Formation of Bicarbonate Species. In forming the PC, the reaction proceeds through a four-centered transition state (**TS2**), cf. Figures 2 and 3; this transition state represents a
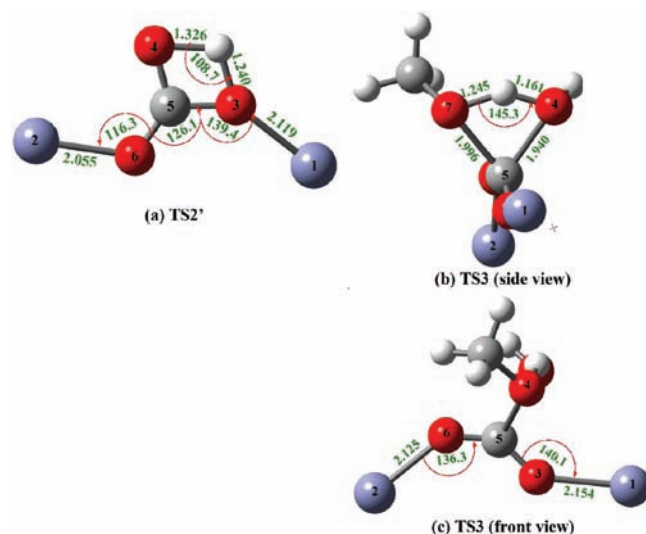
Figure 3. (a) Fragment of TS2; (b) side view of fragment of TS3; (c) top view of fragment of TS3 in the first pathway (bond distances in Å and angles in degree).
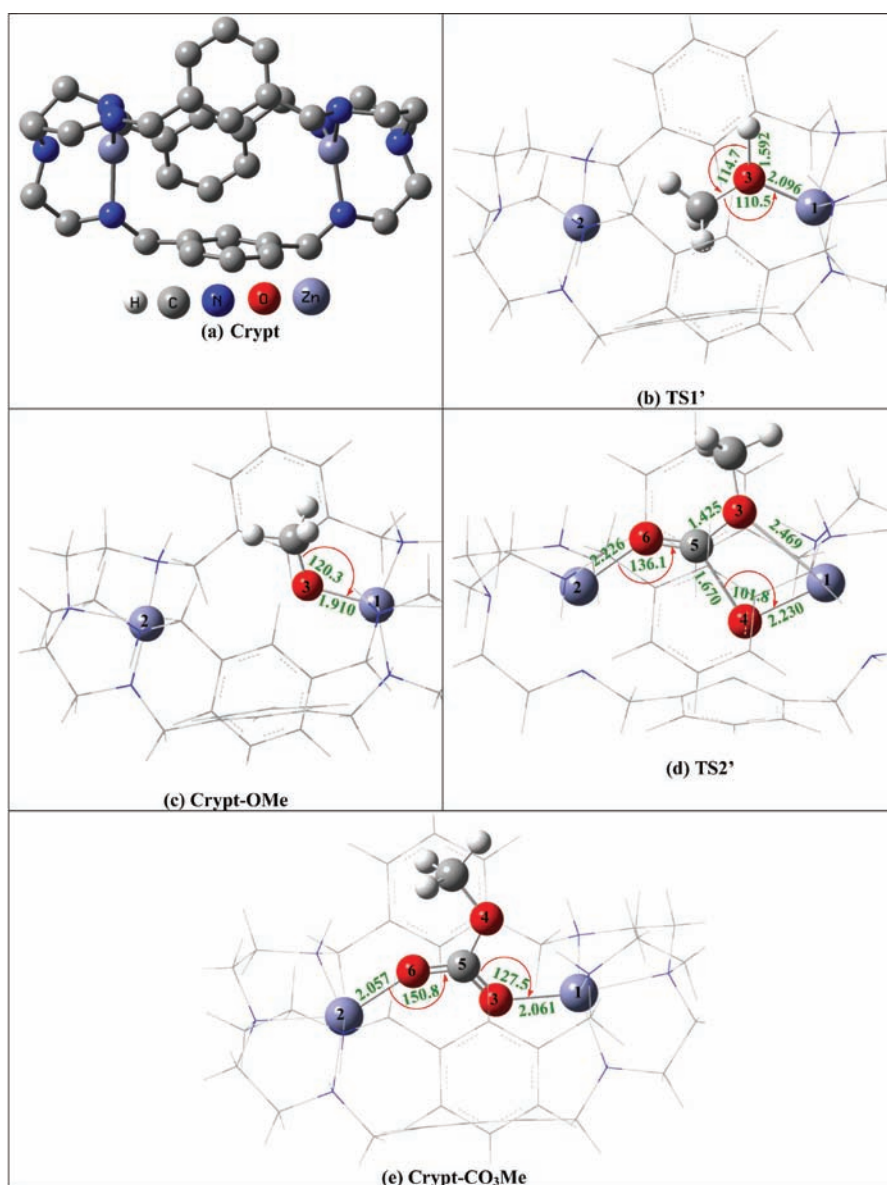
Figure 4. Optimized structures of the reactant, intermediates, transition states, and the product in the second pathway. The atomic labeling of key atoms and bond distances in Å and angles in degree are illustrated on the structures.

nucleophilic attack of metal-bound hydroxide at the electrophilic carbon of CO_2 with concurrent formation of a new bond between the H atom of the Zn-bound hydroxide and the O3 atom of CO_2, leading to proton transfer. Meanwhile, O6 forms a new bond with Zn2. The immediate product from **TS2** is the bicarbonate-cryptate (**Crypt-CO₃H**). The transferred proton is sandwiched between O3 and O4 atoms with O3−H and O4−H distances of 1.240 and 1.326 Å, respectively, and a forming angle (O3−H−O4) equal to 108.7° (as illustrated in Figure 3a). However, the bending of the O−C−O moiety (126.1°) at **TS2** allows a lone pair on the methoxy ligand to point toward an empty sp² orbital of the carbon atom of the CO_2 molecule. It is observed that the group NPA charge on the bound CO_2 fragment in **TS2** and **Crypt-CO₃H** are −0.756 and −0.583 e respectively. This implies that the charge transfer from dinuclear cryptate to CO_2 molecule removes the inactivity of the latter. The NPA charges of O4, C5, and O6 of the bound CO_2 included in **TS2** are 0.786, −0.756, and −0.783, respectively, while those of **Crypt-CO₃H** are 1.057, −0.824,

and −0.816, respectively. By comparison the calculated atomic charge of the free CO_2 atoms (C = 1.014 e, O = −0.507e) at the same level with those of the bound CO_2 in **TS2**, it is observed that the atomic negative charges of C and O atoms increased greatly by *approximately* −0.228 and −0.263 e, respectively.

The optimized geometry of dinuclear zinc carbonato-cryptate, having fixed one CO_2 molecule in the cryptate, is depicted in Figure 2. The included bicarbonate ion between the two zinc cations adopts a *Syn-anti* η_1,η_1 coordination mode forming bis-pentacoordinate around Zn-centers. The O6 atom lies in the plane of the two zinc centers while the rest of carbonate unit lies above it. This reduces the Zn1···Zn2 distance to 5.914 Å. It is clear that the effect of the inclusion of the CO_3^{2-} ion affects the Zn1···Zn2 distance differently than that of a HCO_3^- ion (with the same coordination bond) as the inclusion of a CO_3^{2-} ion reduces Zn1···Zn2 distance *to approximately* 5.163 Å.[6] This supports the Coulombic interaction between the Zn cations and the encapsulated

anion as mentioned before. However, the lengths of Zn1−O3 and Zn2−O6 bonds of **Crypt-CO$_3$H** are 2.071 and 2.045 Å, respectively, which are very close to the experimentally determined bond distances, 1.979 and 1.989 Å, respectively. Also, the structural features of the encapsulated triangular HCO$_3^-$ anion are very similar to those of the free species (calculated at the same level). For example C4−O3, C4−O6, and C4−O5 bond distances of 1.252, 1.263, and 1.373 Å, respectively, are close to those of the free HCO$_3^-$ ion, namely, 1.242, 1.258, and 1.447, respectively. The calculations indicate that the formation of the bicarbonate species is highly exergonic (−29.4 kcal/mol with respect to **PC**). **Crypt-CO$_3$H** is formed by overcoming the **TS2** barrier. It is found that the barrier is very small, and therefore is a highly kinetically favored.

Step (6 and 7): MeOH Attack and Formation of Methoxide Carbonate Species. The final step is the attack of MeOH on the bicarbonate species through a four-centered transition state (**TS3**), cf. Figures 2 and 3. This transition state represents a nucleophilic attack of the hydroxyl oxygen atom of MeOH on the C5 atom of the bicarbonate fragment, with the concurrent formation of a new bond between the H atom of MeOH and one O4 atom of the bicarbonate fragment (subsequently leading to loss of a water molecule to form methoxy-carbonato species (**Crypt-CO$_3$Me**)). For the four-membered **TS3** fragment, O4−H and O7−H distances are 1.161 and 1.245 Å, respectively, while the O4−H−O7 angle is 145°. Long C5−O4 and C5−O7 distances are observed, namely, 1.940 and 1.996 Å, respectively. In the conversion from **TS3** into **Crypt-CO$_3$Me**, the same arrangement occurred. For example, on going from **TS3** into **Crypt-CO$_3$Me**, the C5−O3−Zn1 angle decreased from 140.1° to 127.5°, while the C5−O6−Zn2 angle increased from 136.3° to 150.8°. Meanwhile, Zn1−O3 and Zn2−O6 bond distances reduced by 0.093 and 0.088 Å, respectively. On the other hand, the coordination mode of the CO$_3$Me$^-$ fragment in the **Crypt-CO$_3$Me** cavity adopts the same mode as that of **Crypt-CO$_3$H** molecule, as shown in Figure 2. Based upon these calculations, the relative activation barrier to the transition state **TS3** is 23.7 kcal/mol, characteristic of a kinetically accessible reaction. The formation of **Crypt-CO$_3$Me** is an exergonic reaction compared to **Crypt-CO$_3$** by 5.9 kcal/mol.

Second Pathway. In contrast with the first pathway discussed above, there exists another possible mechanism. This involves four steps: (1) the interaction between the **Crypt** species with one MeOH molecule from the solvation medium to form the first transition state species (**TS1′**), (2) subsequent deprotonation of the complexed MeOH species to form the methoxy species (**Crypt-OMe**), (3) the attack of the **Crypt-OMe** species by a proximate CO$_2$ molecule from the atmosphere to form the second transition state complex (**TS2′**), and (4) the formation of methoxide carbonate species because of the rearrangement of the now attached CO$_2$ molecule (**Crypt-CO$_3$Me**). The energetics of inclusion of a CO$_2$ molecule into the Zn-OCH$_3$ bond of the methoxy species to yield the methoxycarbonato-cryptate is depicted in Figure 5.

Step (1 and 2): Attack of One MeOH Molecule on One of the Zn Ions and Deprotonation. The first step is the attack of one MeOH molecule on the Zn1 cation to form a penta-coordinated center. The optimized structure of this methoxy species (**Crypt-OMe**) is presented in Figure 4. As shown, the methoxy species lies above the plane formed by dinuclear zinc centers, where Zn1−O3−C is 120.3° and the Zn1−O3 distance is 1.910 Å. It is worth mentioning that the
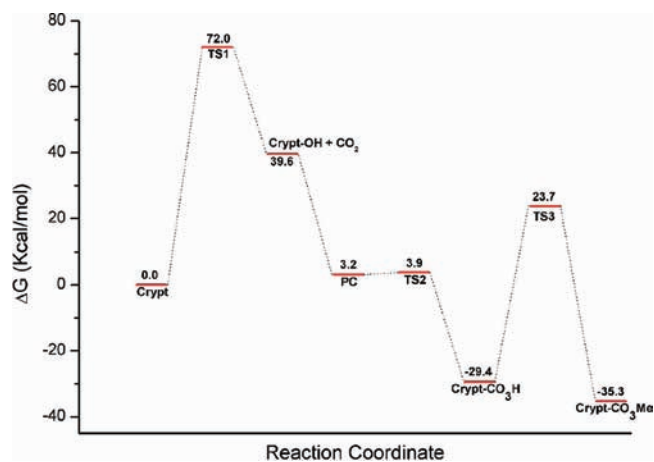
Figure 5. Calculated Gibbs free energy (kcal/mol) profile for the first pathway including the solvation. The values refer to relative Gibbs energy wrt the starting reactants.

Zn1···Zn2 distance is greatly affected by the formation of the methoxy species. Although the Zn···Zn distance of the **Crypt** species is 6.841 Å, it reduces to 6.307 Å in **TS1′**, with a further reduction in **Crypt-OMe** to 6.162 Å. This notable reduction is due to the Coulombic attraction as a result of the proximity of the water's oxygen atom to the activated species. This can been seen from natural population analysis before and after forming the **Crypt-OMe**, wherein the charges on Zn$_9$ and Zn$_{10}$ of **Crypt** are 1.415 e and 1.420 e, respectively, and they decrease to 1.358 and 1.394 e, respectively, after the inclusion of the −OCH$_3$ group in the dinuclear zinc pairing. However, the formation of the methoxy species is relatively endergonic by 37.5 kcal/mol, which is 2.1 kcal/mol less than for **Crypt−OH**. Thus, the formation of the former is a more thermodynamically favorable step than that of the latter. The relative activation barrier to the transition state **TS1′** is 69.6 kcal/mol, which is less by 2.5 kcal/mol than that for **TS1**; thus, the formation of the methoxy species is slightly more kinetically accessible than the formation of the hydroxyl species.

Step (3 and 4): Activation of CO$_2$ and Formation of Methoxide Carbonate Species. Once the methoxy species is formed, it attacks one CO$_2$ molecule to generate a four-centered transition state **TS2′**, where the CO$_2$ molecule interacts with both the Zn1 center and the oxygen atom of the O−CH$_3$ group. Through it, a carbonate bridge is formed where one bond is broken and three new bonds formed. The O4 atom of the free CO$_2$ interacts with Zn1 atom to form a Zn1−O4 bond (2.230 Å) with a concurrent C5−O4 bond formation (1.425 Å). Meanwhile, the Zn1−O3 bond elongates from 1.910 to, a considerable, 2.469 Å. These structural arrangements are sufficient to bring the Zn2 atom close to the O6 atom; to a distance of 2.226 Å, resulting in a methoxycarbonate bridge formation. In this case, the insertion mechanism is not needed as O6 is close to Zn2. For the insertion mechanism, the C−O bond of CO$_2$ interacts first with the metal−oxygen bond, then the bound CO$_2$ rotates to direct the unbound oxygen to the reaction position.[29] In **TS2′**, the C5−O4 distance is closer to the equilibrium distance (by 0.058 Å) than the Zn1−O4 and Zn2−O6 distances (by 0.169 and 0.189 Å). This geometrical feature shows that the driving force for CO$_2$ activation arises from the interaction with the methoxy ligand. However, the dihedral angle of Zn1−O4−O6−Zn2 is

173.0° indicating that the MeCO3⁻ fragment deviates slightly from the plane formed by the two zinc centers.

It is observed that the group NPA charge on the bound CO_2 fragment in **TS2′** and **Crypt-CO₃Me** are −0.754 and −0.599 e, respectively, indicating the role that charge transfer plays a significant role in the activation of CO_2. For example, O4, C5, and O6 of the bound CO_2 included in **TS2′** are 0.786, −0.756, and −0.784 e, respectively, while those of **Crypt-CO₃Me** are 1.033, −0.812, and −0.820 e, respectively. By comparison the calculated atomic charge of the free CO_2 atoms (C = 1.014 e, O = −0.507e) at the same level with those of the bound CO_2 in **TS2′**, it is observed that the atomic negative charges of C and O atoms increased greatly by *approximately* −0.228 and −0.309 e, respectively. However, on the basis of our calculation, this step is exergonic by over 52.0 kcal/mol (Figure.6), indicating that
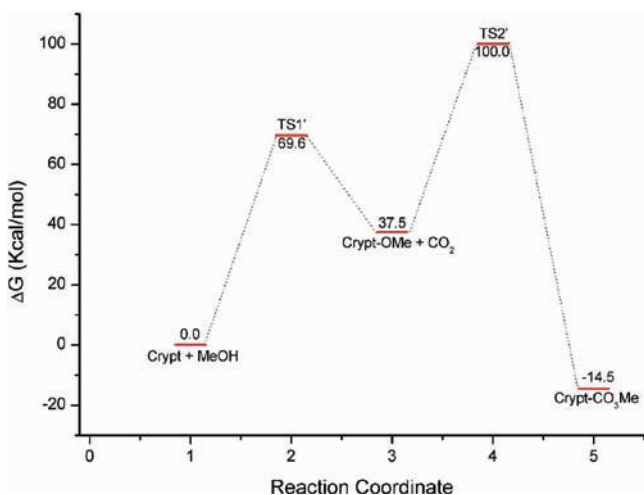
Figure 6. Calculated Gibbs free energy (kcal/mol) profile for the second pathway including the solvation. The values refer to relative Gibbs energy wrt the starting reactants.

the activation of CO_2 is energetically quite stable. The transition state (**TS2′**) is a significant barrier between **Crypt-OMe** and **Crypt-CO₃Me.** The corresponding relative activation barrier is equal to 62.5 kcal/mol, characteristic of a kinetically accessible step. The coordination mode of the CO₃Me⁻ fragment in **Crypt-CO₃Me** cavity adopts the same mode as that of **Crypt-CO₃H** molecule. Interaction of the CO_2 molecule with the Zn-OMe bond of **Crypt-OMe** molecule reduces Zn1···Zn2 greatly by 0.295 Å.

An inspection of the free energy profiles for the pathways investigated suggests that both pathways are possible, with the mechanism proposed by Chen et al.[5] the more likely. We believe that this agrees with the experimental findings obtained by Nelson and co-workers[4] as well as with Chen et al.[5] The former obtained a crystal product of **Crypt-CO₃Me** starting from the **Crypt** (solvating the Crypt species in a mixture of methanol-acetonotrile with one equivalent of preformed carbonate anion under anaerobic conditions) or **Crypt-OMe** species (starting from the **Crypt-OMe** species and reacting under atmospheric conditions). Meanwhile, as already mentioned previously, Chen et al.[5] could react dinuclear copper cryptate in acidic conditions with methanol to form **Crypt-CO₃Me**. However, Chen et al. could not react CO_2 with the methoxy species to form the methylcarbonate; evidenced by the attempt to react it with the mononuclear complex [Cu(tren)-(H₂O)](ClO₄)₂ CH₃OH/CH₃CN (1:1), which did not generate the methylcarbonate species, even when NaOCH₃ was added and the solution left in the open for three days. Taken as a whole, that is, previously reported experiments and the computational results presented here, we suggest that both mechanisms offer feasible routes to CO_2 fixation with that reported by Chen et al.[5] being, on the balance, more likely.

■ CONCLUSIONS

We have investigated two possible reaction mechanisms for the activation of CO_2 catalyzed by a dizinc cryptate. The potential energy profiles were calculated using DFT methods in vacuo and in methanol. On the basis of these DFT computations, we conclude that both mechanisms can be considered as representative models for CO_2 activation in dinuclear cryptate using thermodynamics and kinetic considerations. We can speculate that both pathways can be used to model similar other dinuclear cryptates using different metals like Co^{2+}, Ni^{2+}, Cu^{2+}. However, on balance, the mechanism proposed by Chen et al. offers the pathway with the least free energy penalty.

■ AUTHOR INFORMATION

Corresponding Author
*E-mail: niall.english@ucd.ie.
Notes
The authors declare no competing financial interest.

■ ACKNOWLEDGMENTS

■ REFERENCES

(1) Kitajima, N.; Hikichi, S.; Tanaka, M.; Moro-oka, Y. *J. Am. Chem. Soc.* **1993**, *115*, 5496.
(2) Ruf, M.; Schell, F. A.; Walz, R.; Vahrenkamp, H. *Chem. Ber.* **1997**, *130*, 101.
(3) Lippard, S.J.; Berg, J.H. *Principles of Bioinorganic Chemistry*; University Science Books: Mill Valley, CA, 1994; p 270.
(4) Dussart, Y.; Harding, C.; Dalgaard, P.; McKenzie, C.; Kadirvelraj, R.; McKee, V.; Nelson, J. *J. Chem. Soc., Dalton Trans.* **2002**, 1704.
(5) Chen, J. M.; Wei, W.; Feng, X. L.; Lu, T. B. *Chem.—Asian J.* **2007**, 710.
(6) El-Hendawy, M. M.; English, N. J.; Mooney, D. A. *J. Mol. Model.* **2011**, *17*, 3151−3162.
(7) Darensbourg, D. J.; Lee, W.-Z.; Phelps, A. L.; Guidry, E. *Organometallics* **2003**, *22*, 5585.
(8) Jung, K. T.; Bell, A. T. *J. Catal.* **2001**, *204*, 339.
(9) Sakakura, T.; Choi, J-C; Yasuda, H. *Chem. Rev.* **2007**, *107*, 2365.
(10) Kalhor, M. P.; Chermette, H.; Chambreyb, S.; Ballivet-Tkatchenko, D. *Phys. Chem. Chem. Phys.* **2011**, *13*, 2401.
(11) Tomishig, K.; Ikeda, Y.; Sakaihori, T.; Fujimoto, K. *J. Catal.* **2000**, *192*, 355.
(12) Allen, O. R.; Dalgarno, S. J.; Field, L. D.; Jensen, P.; Willis, A. C. *Organometallics* **2009**, *28*, 2385.
(13) Angamuthu, R.; Byers, P.; Lutz, M.; Spek, A. L.; Bouwman, E. *Science* **2010**, *327*, 313.
(14) Paddock, R. L.; Nguyen, S. T. *J. Am. Chem. Soc.* **2001**, *123*, 11498.

(15) Shen, Y.-M.; Duan, W.-L.; Shi, M. *J. Org. Chem.* **2003**, *68*, 1559.

(16) Arunasalam, V. C.; Baxter, I.; Darr, J. A.; Drake, S. R.; Hursthouse, M. B.; Malik, K. M. A.; Mingos, D. M. P. *Polyhedron* **1998**, *17*, 641.

(17) Srivastava, R.; Bennur, T. H.; Srinivas, D. *J. Mol. Catal. A: Chem* **2005**, *226*, 199.

(18) Vol'pin, M. E.; Koloukov, I. S. *Pure Appl. Chem.* **1973**, *33*, 567.

(19) Kato, M.; Ito, T. *Inorg. Chem.* **1985**, *24*, 504.

(20) Aresta, M.; Dibenedetto, A.; Pastore, C. *Inorg. Chem.* **2003**, *42*, 3256.

(21) Bloodworth, A. J.; Davies, A. G.; Vasishtha, S. C. *J. Chem. Soc. C* (**1967**, 1309.

(22) Davies, A. G.; Harrison, P. G. *J. Chem. Soc. C* **1967**, 1313.

(23) Ghosh, R.; Nethaji, M.; Samuelson, A. G. *Chem. Commun.* **2003**, 2556.

(24) Dibenedetto, A.; Pastore, C.; Aresta, M. *Catal. Today* **2006**, 115.

(25) Ballivet-Tkatchenko, D.; Chermette, H.; Plasserauda, L.; Walter, O. *Dalton Trans.* **2006**, 5167.

(26) Moore, D. R.; Cheng, M.; Lobkovsky, E. B.; Coates, G. W. *J. Am. Chem. Soc.* **2003**, *125*, 11911.

(27) Pandey, K. K. *Coord. Chem. Rev.* **1995**, *140*, 37.

(28) Darensbourg, D. J.; Mueller, B. L.; Bischoff, C. J.; Chojnacki, S. S.; Reibenspies, I. H. *Inorg. Chem.* **1991**, *30*, 2418.

(29) Kalhor, M. P.; Chermette, H.; Ballivet-Tkatchenko, D. *Polyhedron* **2011**, accepted for publication.

(30) Nilsson Lill, S. O.; Köhn, U.; Anders, E. *Eur. J. Org. Chem.* **2004**, 2868.

(31) Liu, Z.; Torrent, M.; Morokuma, K. *Organometallics* **2002**, *21*, 1056.

(32) Kersting, B. *Angew. Chem., Int. Ed.* **2001**, *40*, 3987.

(33) Castro, L.; Lam, O. P.; Bart, S. C.; Meyer, K.; Maron, L. *Organometallics* **2010**, *29*, 5504.

(34) Frisch, M. J.; Trucks, G. W.; Schlegel, H. B., et al. *Gaussian09*, Revision A. 02; Gaussian, Inc.: Wallingford, CT, 2009.

(35) Becke, A. D. *J. Chem. Phys.* **1993**, *98*, 5648.

(36) Lee, C.; Yang, W.; Parr, R. G. *Phys. Rev. B* **1988**, *37*, 785.

(37) Stevens, P. J.; Devlin, F. J.; Chablowski, C. F.; Frisch, M. J. *J. Phys. Chem.* **1994**, *98*, 11623.

(38) Dolg, M.; Wedig, U.; Stoll, H.; Preuss, H. *J. Chem. Phys.* **1987**, *86*, 866.

(39) Glendening, E. D.; Reed, A. E.; Carpenter, J. E.; Weinhold, F. *NBO* 3.1; 2003; Program as implemented in the Gaussian09 package.

(40) Marenich, A. V.; Cramer, C. J.; Truhlar, D. G. *J. Phys. Chem. B* **2009**, *113*, 6378.

(41) Rowland, R. S.; Taylor, R. *J. Phys. Chem.* **1996**, *100*, 7384.